

**Titre:** Experimental methods in chemical engineering: Electron probe  
Title: micro-analysis—EPMA

**Auteurs:** Viviane de Oliveira Campos, Felipe Fernandes Barbosa, Ellen Kadja  
Authors: Lima de Moraes, Dulce Maria Araújo Melo, Jildimara De Jesus  
Santana, & Gregory Scott Patience

**Date:** 2025

**Type:** Article de revue / Article

**Référence:** de Oliveira Campos, V., Barbosa, F. F., de Moraes, E. K. L., Melo, D. M. A., De Jesus  
Citation: Santana, J., & Patience, G. S. (2025). Experimental methods in chemical  
engineering: Electron probe micro-analysis—EPMA. The Canadian Journal of  
Chemical Engineering, 103(7), 3000-3011. <https://doi.org/10.1002/cjce.25712>

 **Document en libre accès dans PolyPublie**  
Open Access document in PolyPublie

**URL de PolyPublie:** <https://publications.polymtl.ca/64695/>  
PolyPublie URL:

**Version:** Version officielle de l'éditeur / Published version  
Révisé par les pairs / Refereed

**Conditions d'utilisation:** Creative Commons Attribution 4.0 International (CC BY)  
Terms of Use:

 **Document publié chez l'éditeur officiel**  
Document issued by the official publisher

**Titre de la revue:** The Canadian Journal of Chemical Engineering (vol. 103, no. 7)  
Journal Title:


**Maison d'édition:** Wiley Blackwell (John Wiley & Sons)  
Publisher:

**URL officiel:** <https://doi.org/10.1002/cjce.25712>  
Official URL:

**Mention légale:** This is an open access article under the terms of the Creative Commons Attribution  
Legal notice: License (<http://creativecommons.org/licenses/by/4.0/>), which permits use, distribution  
and reproduction in any medium, provided the original work is properly cited.

## MINI REVIEW

# Experimental methods in chemical engineering: Electron probe micro-analysis—EPMA

Viviane de Oliveira Campos<sup>1</sup> | Felipe Fernandes Barbosa<sup>1</sup> |  
Ellen Kadja Lima de Moraes<sup>1</sup> | Dulce Maria Araújo Melo<sup>1</sup> |  
Jildimara de Jesus Santana<sup>2</sup> | Gregory S. Patience<sup>2</sup> 

<sup>1</sup>Institute of Chemistry, Universidade Federal do Rio Grande do Norte, Natal, Brazil

<sup>2</sup>Chemical Engineering, Polytechnique Montréal, Montréal, Québec, Canada

## Correspondence

Gregory S. Patience, Polytechnique Montréal, Montréal, QC, Canada.  
Email: [gregory-s.patience@polymtl.ca](mailto:gregory-s.patience@polymtl.ca)

## ABSTRACT

Electron probe microanalysis (EPMA) is a non-destructive spectroscopic technique to map the chemical composition—quantitative elemental distribution and layer thickness—with a micro-scale resolution. An electron beam illuminates the surface of a sample and produces backscattered electrons (BSE), secondary electrons (SE), characteristic X-rays, and light known as cathodoluminescence (CL). Combining energy dispersive spectrometry with wavelength-dispersive spectrometry improves trace analysis and differentiates overlapping X-ray lines, but the detection threshold is not much better than 100 ppm (parts per million). Implementing Monte Carlo simulation with better electronics and software are ongoing research areas to improve the method's precision, sensitivity, and spatial resolution. To detect Li, Be, and B ( $Z < 11$ ) requires wavelength-dispersive X-ray spectroscopy (WDS), or soft X-ray emission spectroscopy (SXES), or a combination of BSE/EDS method. Researchers in metallurgy & metallurgical engineering, mineralogy, geochemistry & geophysics, and mining & mineral processing apply the method most. Chemical engineering is ranked 21st among the 250 scientific categories that use the technique. It is also applied to reconstitute works of art and the antiquities. A bibliometric map identified four clusters of research and for each cluster the major nodes were: (1) geochemistry, (2) mechanical properties, microstructure, and alloys, (3) Fe, Cu, and Cr, and (4) phase equilibria.

## KEYWORDS

backscattered electrons, chemical composition, electron probe microanalysis, elemental distribution, X-rays

## 1 | INTRODUCTION

Electron probe microanalysis (EPMA, also less frequently known as electro microprobe analysis [EMPA]) is an in-

situ non-destructive spectroscopic method to identify and measure a solid material's elemental spatial distribution. It is based on the physical principles of X-ray spectrometry and electron-stimulated X-ray emission.<sup>[1]</sup> A focused

This is an open access article under the terms of the [Creative Commons Attribution](#) License, which permits use, distribution and reproduction in any medium, provided the original work is properly cited.

© 2025 The Author(s). *The Canadian Journal of Chemical Engineering* published by Wiley Periodicals LLC on behalf of Canadian Society for Chemical Engineering.

electron beam interacts with a solid sample to produce backscattered electrons (BSE), secondary electrons (SE), characteristic X-rays, and light known as cathodoluminescence (CL).<sup>[2,3]</sup> The brightness of the greyscale high-resolution images produced by BSE is proportional to the mean atomic number at each pixel and it identifies phases. The SE has a greater sensitivity to surface topography generated near the surface of the sample. X-rays map the element's spatial distribution and CL signals establish the phases of the elements and compounds and estimates the phase distribution and proportions, trace element compositional variation, and surface textural properties of multi-phase composites.<sup>[3]</sup>

When equipped with a wavelength-dispersive spectrometer (WDS), it produces a spectrum of peaks to identify elements. A single measurement may require dozens of parameter adjustments, which adds complexity to the EPMA quantification process and data interpretation. Therefore, to achieve a sufficient exactitude requires a detailed measurement framework.<sup>[4,5]</sup>

Over the past three decades, EPMA has been established as a distinctive technique in the microchemical analysis of materials. It all began experimentally with Moseley in 1913, who discovered a general relationship between an element's X-ray emission lines and its atomic number and suggested that it might be possible to identify the presence of an element based on the X-ray emission spectrum generated by electron bombardment.<sup>[6]</sup>

Castaing and Guinier returned to this investigation in 1949 when they proposed an electron microprobe as a tool.<sup>[7,8]</sup> Castaing included a solid theoretical formulation for quantitative chemical analysis and the specifics of the device they had constructed in his doctoral thesis, submitted in 1951. Cosslet and Duncumb increased the equipment's adaptability by adding the capacity to scan electron beams.<sup>[6]</sup>

Despite significant advances in technology and equipment, the components of an electron probe microanalyzer remain fundamentally the same, although their operating efficiency has been greatly improved. The sensitivity of either wavelength-dispersive or energy-dispersive spectrometers reaches a sensitivity of 1–100 ppm for elements from Be to U and an accuracy of < 2% when the mass fraction is >10% (material dependent). Internal shielding has expanded the instruments capability to include actinides up to Cm.<sup>[6,9]</sup> Other developments—WD parallel beam spectrometry, soft X-ray emission spectrometry (SXES), and windowless ED spectrometry—broadened its capability for light elements analysis defined as Li to F.

Previous reviews have detailed EPMA's fundamentals, applications, analytical methods, and instrumentation methodology. This tutorial review is part of a series

dedicated to experimental methods and applications specific to chemical engineering.<sup>[10]</sup> Some of the more recent articles in the series cover both modelling (CFD/finite volume method, data processing and data usage in decision-making, and Monte Carlo simulation)<sup>[11–13]</sup> and spectroscopic techniques (XRF).<sup>[14]</sup> Here we highlight applications across diverse technological domains and spotlight recent advances. According to the classification of chemical engineering techniques, EPMA is in the bottom quartile and is seldom mentioned in *The Canadian Journal of Chemical Engineering*.<sup>[10]</sup>

## 2 | THEORY

### 2.1 | Principles, electronic components, and function

An EPMA instrument comprises an electron gun (filament or tip – 2 in Figure 1) to generate an electron beam (3) that travels through apertures (5, 7) and lenses (6) and then interacts with the sample (13) on a stage (12) to generate X-rays and electrons, which are analyzed with EDS, WDS, BSE, SE, and IR detectors located around the sample chamber (Figure 1).<sup>[15,16]</sup> The electron gun (electron source) is usually a tungsten filament (or tip) or a cone-shaped tungsten cathode that generates thermionic emission (Figure 1–

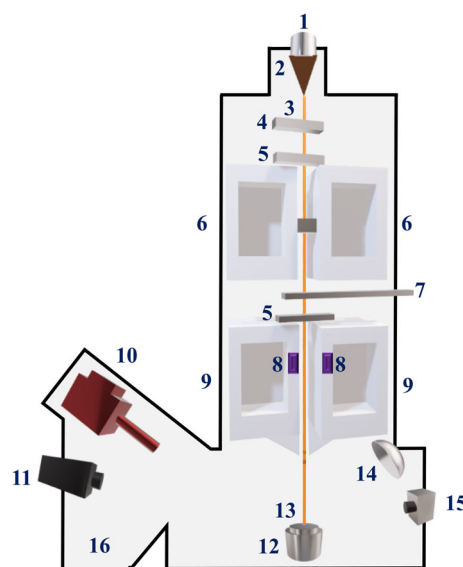


**FIGURE 1** Main components of electron probe microanalysis (EPMA) equipment, where: (1) high-voltage cable, (2) filament or tip, (3) electron beam, (4) anode, (5) spray apertures, (6) condenser lens, (7) adjustable aperture, (8) scanning coils, (9) objective lens, (10) energy dispersive X-ray detector, (11) secondary electron detector, (12) stage, (13) sample, (14) backscattered electron detectors, (15) infrared camera, and (16) high vacuum/pumps.

1,2).<sup>[15,17]</sup> Larger electron beams reduce scan time at the expense of resolution, which reaches a magnification of  $400,000\times$ . Anode positively biased plates (4) accelerate low-energy electrons generated from the cathode to energies between 3 and 30 keV.<sup>[18]</sup> The emission density,  $i_0$ , increases proportionately with its material constant  $A$  and the square of temperature  $T$  (in Kelvin)<sup>[17,19]</sup>:

$$i_0 = AT^2 \exp - \frac{B}{kT}, \quad (1)$$

where  $B$  is directly proportional to the material's work function that makes up the filament, and  $k$  is Boltzmann's constant. The electron penetration depth,  $d$ , is proportional to the voltage and acceleration,  $V$ , and inversely proportional to the atomic number,  $Z$ , and the incidence angle,  $\theta$ <sup>[20]</sup>:

$$d = \frac{V}{Z \cdot \cos \theta}. \quad (2)$$

The electron optics system, similar to light optics, uses a set of electromagnetic lenses placed in the instrument's column to condense and focus the electron beam released from the source. The sample stage has a moveable platform ( $X - Y - Z$ ). It operates under vacuum to minimize gas and vapour molecules from interfering with the electron beam pointed at the sample. Additionally, the resulting nearly  $1\mu\text{m}$  diameter electron beam for a W filament (that is as small as 10 nm for a W tip) shines on the entire sample or on specific spot, resulting in cathodoluminescence, phonon excitation, continuum X-ray radiation (bremsstrahlung), Auger electron production, characteristic X-ray radiation, secondary electrons, and backscattered electron production.<sup>[15,18]</sup>

In WDS, an electron beam strikes the sample generating characteristic X-rays (15–20 keV). An analytical crystal with a specific lattice spacing directs (reflects) the X-rays of a determined wavelength to either a gas proportional counter or sealed proportional counter detector. The broad polychromatic X-ray from the single crystal follows the Bragg equation<sup>[21]</sup>:

$$n\lambda = 2d_{\text{Bragg}} \sin \theta, \quad (3)$$

where the lattice spacing,  $d_{\text{Bragg}}$ , is known, the angle,  $\theta$  between the X-ray beam, and the surface of the material is varied continuously while acquiring a spectrum (but set to a fixed value when measuring a characteristic X-ray line energy or background energy) and the product of the wavelength,  $\lambda$ , and the diffraction order,  $n$  is determined.

The final step is to correct for matrix effects due to atomic number ( $Z$ ), absorption ( $A$ ), and fluorescence ( $F$ ).<sup>[9,22]</sup> To capture the entire spectrum requires adjusting the angle the light strikes the crystal repeatedly.<sup>[18,22]</sup> To focus X-rays requires that the sample, crystal, and detector must lie on the Roland circle as the position of the crystal relative to the sample changes.

An energy dispersive spectrometer (EDS) is a solid-state semiconductor detector that accumulates X-rays of all wavelengths produced from the sample and efficiently and concurrently records X-rays throughout the whole energy range. EDS has lower energy resolution than WDS, and overlaps between X-ray lines are more common, requiring peak deconvolution to extract X-ray intensities.<sup>[9,18,22]</sup>

The EPMA technique is comparable to TEM and SEM,<sup>[15,23]</sup> but includes an optical microscope for WDS spectrometers to analyze specific regions. One of the comparative advantages of the EPMA is that drifting and fluctuations of the electron beam current are lower as some the electron beam is stabilized with an active feedback loop. EPMA's image in variable energy ranges and beam diameters makes it more sensitive than SEM's EDS detector for multi-element analysis. A multichannel plate detector linked to a TEM is necessary to achieve a spectral range of  $\approx 32\text{ eV}$ .<sup>[23,24]</sup>

For quantitative analyses, an electron beam is focused on a specific point. Then, the intensity of the sample's characteristic X-ray lines of the elements is compared to standards of known composition, and any differences in matrix effects between the sample and standard are adjusted for. The approach employs typical  $ZAF$  or  $\phi(\rho z)$  correction processes and compares the unknown sample's X-ray intensity with that of the reference material. This step is required since matrix effects can modify the X-ray generation and/or increase X-ray emission intensity (depending on the standard) compared to reference standards. Consequently, the maximum analytical spatial resolution—defined as the smallest volume that enables accurate chemical analysis—is determined by the extent of electron beam scattering within the target. As a result, the maximum analytical spatial resolution (i.e., the lowest volume that yields a precise chemical analysis) is determined by the spread of the electron beam inside the target.<sup>[9]</sup>

One of the challenges is achieving outcomes regarding soft elements since their energy is less than 1 keV. One approach is to use a soft X-ray emission spectrometer (SXES), which provides high spectral resolution with energy ranges of 100–2300 eV with varied line spacing grating, and high detection sensitivity. Besides that, SXES identifies chemical shifts, phase and determines C and N abundances and chemical bonding state.<sup>[25,26]</sup>



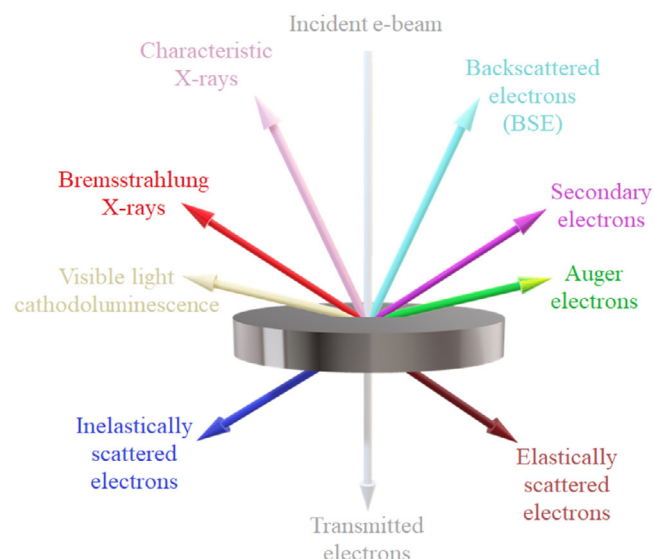


**FIGURE 2** Electromagnetic radiation produced when an electron beam shines on a sample.

When the electron beam strikes the sample, a fraction of the incident beam is absorbed, some traverses the sample and scatters, and other produces X-ray and cathodoluminescence (Figure 2). The type of electromagnetic radiation generated depends on the morphology and elemental composition of the sample.

SE from inelastic events and BSE from elastic events are the source of radiation to produce SEM images (1 nm depth from SE and 1  $\mu\text{m}$  from BSE).<sup>[15]</sup> The size of the electron interaction volume is a function of the composition of the material and the accelerating voltage, which can be characterized with Monte Carlo simulation, especially for heterogeneous samples.<sup>[13]</sup> Monte Carlo models estimate electron transport and approximate the measured X-ray intensity. However, statistical noise restricts these estimates.<sup>[9,13,27]</sup>

When the electron beam excites the sample, it emits characteristic X-rays for which the WDS and EDS detectors assign its elemental composition. The concentration of an unknown species is the product of the ratio of the intensities of the unknown element to a standard ( $k = I_{\text{unk}}/I_{\text{std}}$ ) and the concentration of the standard  $C_{\text{std}}$ <sup>[28,29]</sup>:

$$C_{\text{unk}} = k \times C_{\text{std}} \times \frac{ZAF_{\text{unk}}}{ZAF_{\text{std}}}, \quad (4)$$

where  $ZAF$  is the correction factor for the non-linear relationship between an element's concentration and X-ray intensity (Castaing's approximation) and  $Z$  corrects for atomic number,  $A$  corrects for absorption, and  $F$  corrects for fluorescence.

In the interaction of the electron beam with atoms, electrons are emitted from an inner layer quickly filled by electrons from outer layers, releasing energy in this transition that is transferred to another electron being ejected from the atom; the second ejected electron is called an Auger electron. An Auger electron detector is sensitive for light elements (for most elements at 0.01–0.1%, atomic), that is, low atomic mass, and characterizes the material's surface chemical (elemental) composition.<sup>[30]</sup>

When an electron beam interacts with a phosphor, it generates visible and ultraviolet light—cathodoluminescence (CL): an electron from the valence band is excited to the conduction band and emits a photon with a characteristic wavelength (colour). A CL image identifies mineral phases,<sup>[31]</sup> composition, morphology, and structural and microstructural defects by grey contrast (according to the atomic number).

### 3 | APPLICATIONS

Because of its versatility, researchers from material sciences, mineralogy, chemistry, physics, archaeology, and engineering apply EPMA to map out species spatial distribution. Besides R&D, EPMA contributes to quality control, and conservation and restoration (Figure 3). The technique is expanding its analytical capabilities with additional spectroscopic technology. Further improvements in resolution will help expand into chemical engineering as it is seldom applied at this time.



**FIGURE 3** Main applications, challenges, and advances in EPMA.

The Web of Science Core Collection has indexed 1500 articles that mention EPMA from 2021 to 2023. Of the 250 scientific categories in the database, journals in 66 categories mention the technique at least twice. The most prolific categories are multidisciplinary materials sciences with 696 occurrences, followed by metallurgy & metallurgical engineering (585 occurrences), mineralogy (315), geochemistry & geophysics (254), and mining & mineral processing (214). Chemical engineering is ranked 21st with only 26 articles that mention EPMA.

EPMA is ideal to detect the presence of minerals in rocks, and identifying mineral phases. Geologists and geochemists apply elemental mapping to facilitate rapid analysis, characterize how rocks form and evolve with time, identify host minerals with valuable elements, and assess purity. Modern instruments have lower detection limits, which decrease the uncertainty in evaluating the economic viability for mineral extraction.<sup>[32,33]</sup>

To identify the main research thrusts, we created a keyword bibliometric map from Web of Science with

VOSviewer (Figure 4).<sup>[34,35]</sup> VOSviewer grouped the 100 most often mentioned keywords into four clusters. The red cluster centres around geochemistry and evolution (with EPMA close to the centre of the map). The green cluster has the 2nd most keywords after the red cluster in which mechanical properties, microstructure, and alloy, are the most prominent keywords. The blue cluster has the third most keywords and the subjects deal mostly with the metals Fe, Cu, Zn, Cr. Finally, the dominant subject of the yellow cluster, is phase equilibria but it also contains nodes representing elements that are in the vicinity of the blue cluster, namely Ni, Al, and Mg.

### 3.1 | Catalysis

EPMA would seem ideal to study catalytic systems as it identifies phases, elemental composition, and distribution, but only 22 of the 1700 articles in the database mention catalyst or catalysis. It characterizes active metals on

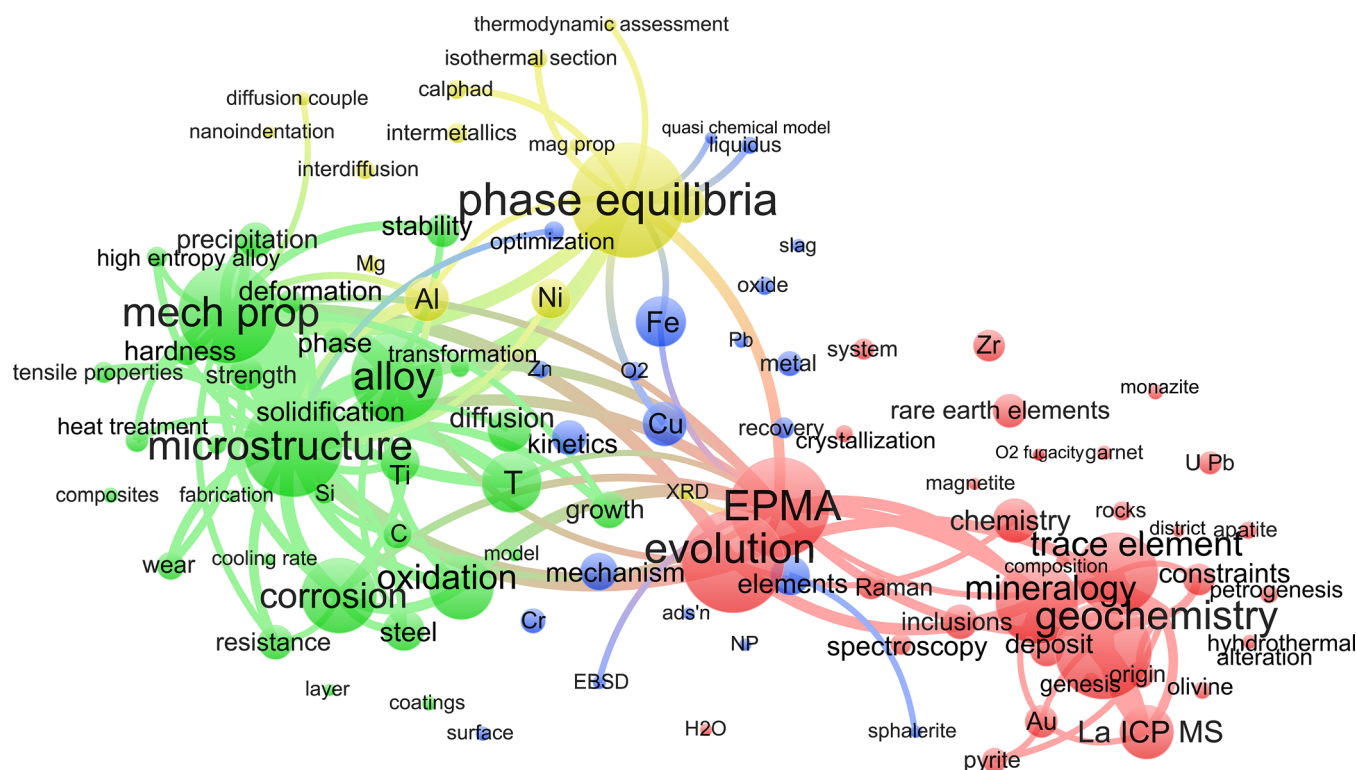


**FIGURE 4** EPMA bibliographic map of the 100 most mentioned keywords in the > 1700 articles indexed by Web of Science from 2021 through to mid 2024.<sup>[34,35]</sup> The node size is proportional to the number of articles that mention the corresponding keyword: The smallest nodes represent 18 articles, while the largest (phase equilibria) represents 174 articles. The keywords microstructure, mechanical properties, and EPMA all had more than 174 mentions (273, 218, and 197, respectively), but to minimize overlap between nodes, we assigned a value of 150 to these keywords. The red cluster has 34 keywords and EPMA has the most mentions at 197, The green cluster has 32 keywords and the most frequently cited is microstructure at 273, The blue cluster consists of 21 nodes and Fe is mentioned 75 times, and there are 14 keywords in the yellow cluster and phase equilibria is mentioned 174 times. Lines in the map represent how often the articles are cross referenced.

ads'n—adsorption, EBSD—electron backscatter diffraction, mag prop—magnetic properties, mech prop—mechanical properties, NP—nanoparticle, and  $T$ —temperature.

heterogeneous surfaces in a single analysis and generates a colour map for each element to quantify how well they are dispersed, which is an essential characteristic to assess activity and detect phenomena like sintering that deactivates catalyst (Figure 5). In the case active sites are too close together, adsorbed reactants interact and restrict desorption or react to form larger molecules (like coke), which restricts access to activate sites by blocking pores and is another deactivation mechanism.<sup>[36]</sup>

WDS-EPMA and EPMA combined with other complementary techniques map light elements ( $Z < 11$ ), which are problematic for EDS-EPMA.<sup>[37–39]</sup> Auger, for example, is capable of detecting Be. AFM is a competitive analytical technique but could be a complementary technique.<sup>[40]</sup>

Liu et al. investigated the surface of a commercial Phillips  $\text{CrO}_x/\text{SiO}_2$  catalyst interacting with ethylene at room temperature with EPMA.<sup>[41]</sup> They found that Cr islands formed of varying sizes and the number of active Cr species decreased during reaction.

Wang et al. investigated the monolithic ZSM-5 @ nano-ZSM-5 catalyst printed in 3D by EPMA, to characterize the elemental distribution of Si and Al.<sup>[42]</sup> They identified a very Si rich region 30  $\mu\text{m}$  thick indicating ZSM-5 crystallizes on the surface. In the case of the elemental composition of an S-FeCoO catalyst, both EPMA (EDS) and ICP micrographs demonstrated that Fe, Co, S, and O were highly dispersed on the surface.<sup>[43]</sup>

Dao et al. investigated by EPMA a heterogeneous catalyst consisting of Pt with varying levels of S, applied to the dehydrogenation of perhydro-benzyl-toluene.<sup>[44]</sup> The

morphology of the material was analyzed, as well as a quantitative WDS analysis of the elements present. The profile in the micrograph indicated that Pt was impregnated into the  $\theta\text{-Al}_2\text{O}_3$  spheres, resulting in a core-shell structure, while the subsequent addition of S caused part of the platinum to migrate into the structure, leading to a uniform distribution.

Images generated by backscattered electrons and elemental distribution maps by WDS and EDS confirmed the presence of the main metals Al, Ce, and Zr, in addition to P, Ca, S, Ba, and O on the surface of aged automobile exhaust catalyst.<sup>[45]</sup> Pd and Rh precious metals (in smaller quantities) were highly dispersed, favouring an improved efficiency to convert exhaust gas pollutants, while also resisting forming alloys. The EPMA images showed that a layer of mixed phosphates containing Ca and Zn cations formed, sulphur reacted to aluminium sulfate, and the metal particles sintered due to the high temperature.

Other tests over catalytic converters indicated that concentrations of Pd, other noble metals, and rare earth varied along the length: Pd and Rh migrated from the inlet to the outlet (due to diffusion induced by the temperature gradient along the axis).<sup>[3]</sup> The trend was similar for C, N, and P impurities as they also deposit at the exit where the temperature is  $> 100^\circ\text{C}$  lower than at the inlet. Conversely, S was enriched at the inlet.

### 3.2 | New materials and metal alloys

EPMA is ideal to determine the chemical composition of metal alloys including their elemental and concentration distribution. Besides R&D, engineers and scientists characterize the type of corrosion on surfaces and alloy/material quality based on composition.

In the Al-Si quasi-eutectic alloy, Ca is an impurity that enters the composition from the Si source.<sup>[46]</sup> It enhances  $\alpha\text{-Al}$  and Si dendrites formation in the alloy structure. The EPMA analysis for this material (Figure 6), identified how Ca and O were distributed in Al and Si: They formed a hypo-eutectic structure with  $\alpha\text{-Al}$  and Si dendrites.

In a cast Al-Si-Cu alloy, EPMA mapped the distribution of transition metals (Zr, V, and Ti) to identify materials with the best mechanical performance at high temperature.<sup>[47]</sup> Segregation profiles of Zr, V, and Ti elements in the material's FCC matrix were evaluated with the Sheil model (Figure 7). Despite differing profiles, there is a tendency for transition metal elements to segregate towards dendritic centres. Thus, the best material for high-temperature resistance

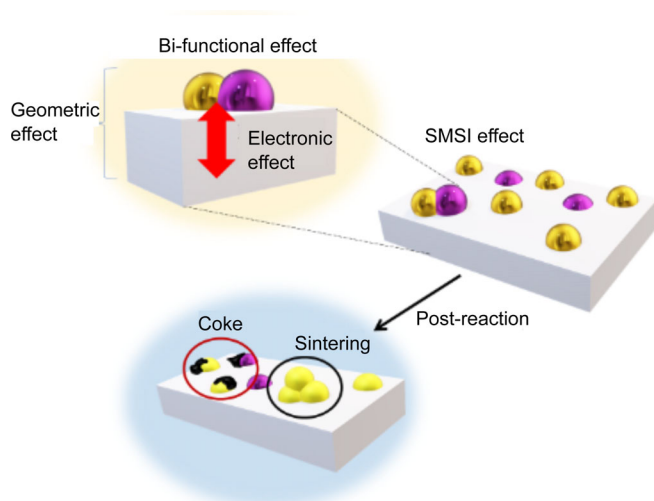


**FIGURE 5** Main observations made with an EPMA analyzer involving catalysis: Metal identification, distribution of active sites (metals), strong metal support interaction (SMSI) effect, identification of coke or other impurities after reaction and sintering.



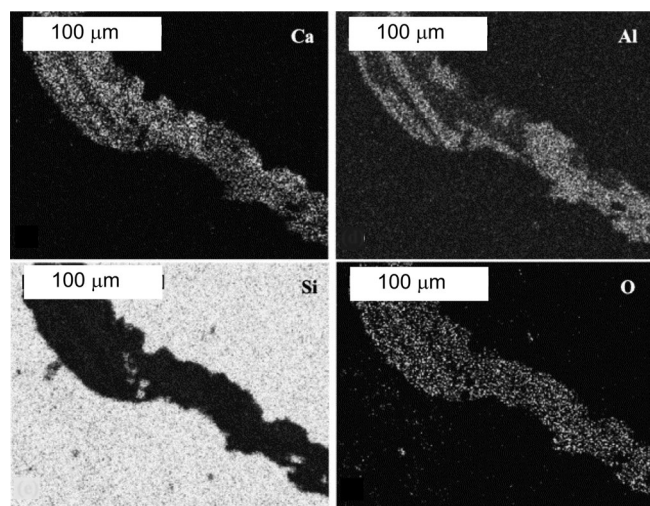


FIGURE 6 EPMA mapping of calcium and oxygen impurities in Al-Si alloys, highlighting the formation of  $\alpha$ -Al and Si dendrites. Adapted from Liu et al.<sup>[46]</sup> Copyright Elsevier.

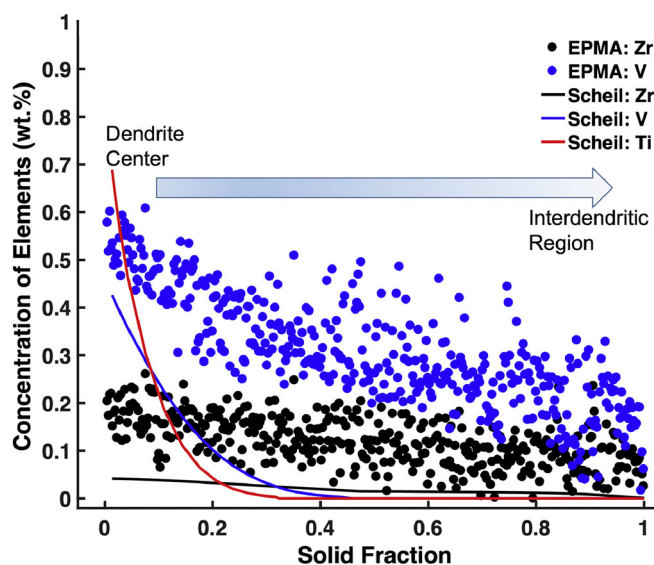


FIGURE 7 Segregation profiles of Zr and V in Al-Si-Cu alloy with the Scheil model predictions. Adapted from Cheng et al.<sup>[48]</sup> Copyright Elsevier (2015).

exhibited nanoscale precipitates, making these materials appealing for use in automotive engines.

Cheng et al.<sup>[48]</sup> investigated inter-granular corrosion of an alloy consisting of Ni–Mo–Cr–Fe in a tellurium atmosphere at 800°C. After 100 h at 800°C, the alloy corroded with Te on the surface and reaching approximately 110  $\mu\text{m}$  below the surface. This suggests that Te diffuses in the alloy along the grain boundaries (inter-granular diffusion). The formation of a cubic CrTe structure may propagate inter-granular cracks in the alloy (Figure 8).

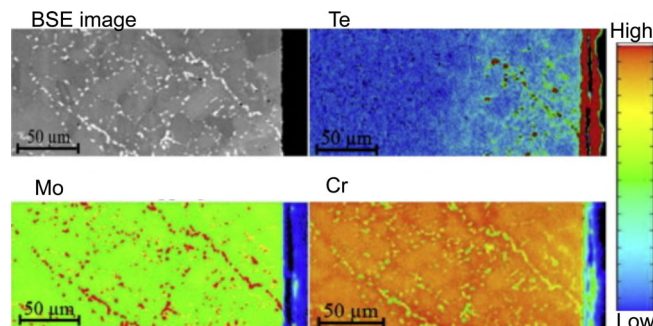


FIGURE 8 Backscattered and EPMA images of Ni-Mo-Cr-Fe alloy corrosion in a Te atmosphere. Adapted from Liu et al.<sup>[46]</sup> Copyright Elsevier (2005).

### 3.3 | Geology and mineralogy

Geological and geochemical knowledge of the nature of minerals is critical for mineralogists and process metallurgists to determine how rocks form and evolve with time, identifying valuable elements in a host mineral, and verifying purity (homogeneity). The technique is currently widely applied in geochronology, aiming to measure isotopic concentrations of chemical elements in minerals, correlating them with the calculation of radiometric age. As the vast majority of mineral samples have several phases, element mapping provides a rapid analysis for characterizing these samples, as well as a notion of the % of these elements by EDS and WDS.<sup>[32]</sup> Based on a thorough analysis of the minerals, geologists estimate, in economic terms, the feasibility of exploiting certain minerals.

Despite being well-established in geology, the remaining challenges include precision and accuracy.<sup>[49]</sup> Due to the sensitivity of geological matrices to electron beam irradiation, there is a loss of X-ray intensity over time. The effects of certain alkaline elements during electron beam bombardment have been investigated for decades to improve quantification precision.<sup>[5]</sup>

Eren and Palvanov investigated the chemical composition of a sample of calcite (CaO) that fills a stalagmite in the Küpeli cave in Turkey.<sup>[50]</sup> Initially, the dendritic character of the grains was identified from a morphological analysis (images obtained by backscattering), which indicated that calcite is predominant in the stalagmite, at around 56%, with traces of Na<sub>2</sub>O, MgO, SiO<sub>2</sub>, SrO, MnO, Al<sub>2</sub>O<sub>3</sub>, K<sub>2</sub>O, FeO, and BaO. The expected minerals therefore consist of feldspar, chlorite, haematite, quartz, and calcite. The presence of organic material in some of the pores investigated suggests factors that may influence the mineralogical formation mechanisms of the stalagmite.



Tainiolite, discovered in the Kaerqiaer belt in north-west China, is a potential source of F and Li ores.<sup>[51]</sup> EPMA analysis showed that the tainiolite had high concentrations of Li, Rb, Cs, Sn, and Nb and low concentrations of Ta from which they derived the average crystalline formula:  $K_{0.93}Li_{1.11}Mg_{2.16}Fe_{0.14}Ti_{0.01}(Si_{3.52}Al_{0.34}O_{10}OH_{0.08}F_{1.92})$ . Due to the limitation of EPMA to quantify hydroxides, it was inferred from correlations based on the charge balance.

Ilmentie was detected off the southern coast of Brazil and Wust et al. applied EPMA to identify the composition<sup>[52]</sup>:  $TiO_2$  (0.55 g g<sup>-1</sup>),  $FeO$  (0.39 g g<sup>-1</sup>),  $MnO$  (0.013 g g<sup>-1</sup>),  $MgO$  (0.011 g g<sup>-1</sup>),  $Al_2O_3$  (0.005 g g<sup>-1</sup>), and  $SiO_2$  (0.004 g g<sup>-1</sup>). Trace impurities (> 0.001 g g<sup>-1</sup>) included:  $CaO$ ,  $NiO$ ,  $P_2O_5$ ,  $Cr_2O_3$ , and  $K_2O$ . Backscattered electron images, with varying shades of grey on the grains identified  $TiO_2$  content and degree of alteration.

### 3.4 | Conservation and restoration

Through multidisciplinary collaborations, archaeologists, anthropologists, historians, and scientists (physicists, chemists, and engineers), apply EPMA to meticulously investigate ancient artefacts and works of art. For example, they determine the chemical composition of paint pigments to better identify the shade closest to the original or determine how that paint was produced. This is particularly pertinent when examining forged pieces made from bronze and other alloys, or even of vases and porcelain as it reveals how they were manufactured. In a certain way, the chemical composition of materials serves as a critical indicator of interactions between ancient civilizations.<sup>[53–55]</sup>

## 4 | UNCERTAINTY, ACCURACY, AND DETECTION LIMITS

The cost of an EPMA instrument ranges between \$500,000 and \$2,000,000, depending on specifications, features, and manufacturer. Operating this advanced instrument requires specialized training provided by the manufacturer and a solid professional background in science or engineering. Sample preparation generally takes 30–40 min, depending on the sample type. The process involves cutting and polishing (to create a flat surface), applying a chemical coating to prevent surface charging, and ensuring the sample is compatible with vacuum conditions and the electron beam to minimize damage or interference. Reaching the required vacuum typically takes 10–40 min.

The time required for analysis depends on the sample's complexity and the application, such as the number of elements to be detected. Analysis ranges from half an hour to several hours. Despite the high costs associated with the equipment and its operation, the results are invaluable when adequately conducted, delivering highly sophisticated, detailed, and reliable analytical insights. The high counting rate, driven by the high intensity of the beam current, improves the detection limits, accuracy, and precision. A WDS spectrometer counting the number of X-rays passing through the crystal at a specific angle achieves precise quantitative analysis.

The analytical spatial resolution (the region from the X-rays emanate) is proportional to the beam diameter. For any X-ray line, resolution improves working at low overvoltage—ratio of the electron beam energy to the critical ionization energy.

The accuracy and precision of EDS analyses are comparable to WDS analyses, provided that the element exceeds the minimum threshold, which depends on the nature of the sample, the element, and the counting duration. The detection limits for a 100 ms dwell time are between 0.0005 and 0.0026 g g<sup>-1</sup> (0.26% by mass) of elements.<sup>[56,57]</sup>

For quantitative analysis, X-ray maps rely on internal standards, and a calibrated map typically contains approximately 312,000 pixels. This number refers to a standard map size (e.g., 600 × 520 pixels) to illustrate the typical dataset acquired during analysis. In traditional analysis, each pixel on the map is individually quantified using *ZAF* or  $\phi(\rho z)$  correction methods.<sup>[58]</sup>

For phases in mineralogical samples, EPMA reaches an average analytical precision for a single garnet pixel composition of 0.028 g g<sup>-1</sup> for Si and 0.2 g g<sup>-1</sup> for Mg. Averaging the composition of multiple homogeneous pixels improves precision, enabling the detection of subtle compositional zoning. For example, averaging over a 10 × 10 μm<sup>2</sup> square window reduces the mean analytical uncertainty of the garnet composition to 0.0028 g g<sup>-1</sup> for Si and 0.02 g g<sup>-1</sup> for Mg.<sup>[59]</sup>

Old car exhaust catalysts contain dispersed elements such as P, Pt, and Zr, which are challenging to determine with EDS alone due to overlapping energy peaks around ≈ 2 keV. A WDS spectrometer identifies traces of Pd and Rh (Figure 9).<sup>[45]</sup> By integrating EDS and WDS, EPMA achieves comprehensive trace element determination in a single assay. For example, EDS spectral lines *K α* of P and *L α* of Zr overlap, which compromises the results but are clearly differentiated with WDS (Figure 10).<sup>[45]</sup> Since WDS has an energy resolution of approximately 10 eV, it provides better precision for analyzing these elements

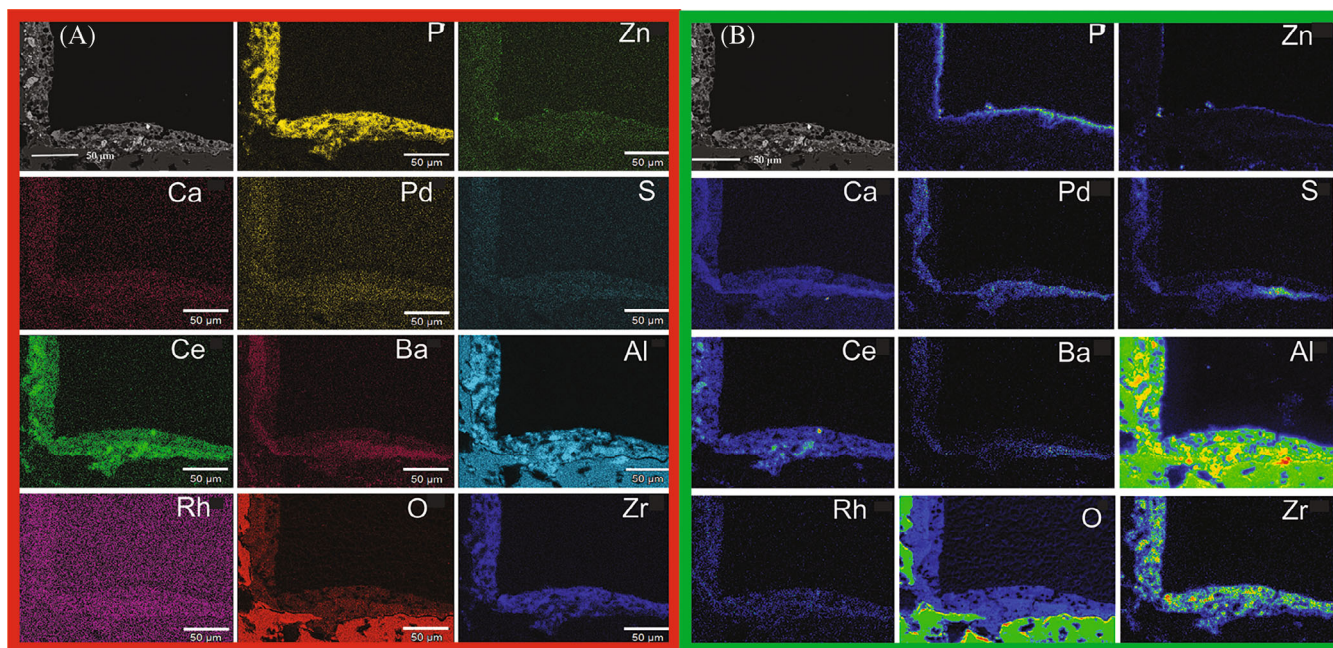


**FIGURE 9** Elemental mapping of the cross-section of used automotive exhaust honeycomb: Red: 12 images to the left in square A: EPMA-EDS, green: 12 images to the right in square B: EPMA-WDS. For the Pd, Rh, and S images, the EDS identifies a slight outline of the elements but includes a significant background, whereas the WDS images more clearly demarcates the elements from the background and the Al substrate. The P, Ba, and Zn images are smeared in the EDS image (right) while the WDS image shows highly concentrated lines along the edge of the honeycomb. The images are essentially equivalent for the other elements. Adapted from Bian et al.<sup>[45]</sup> Copyright Elsevier (2024).

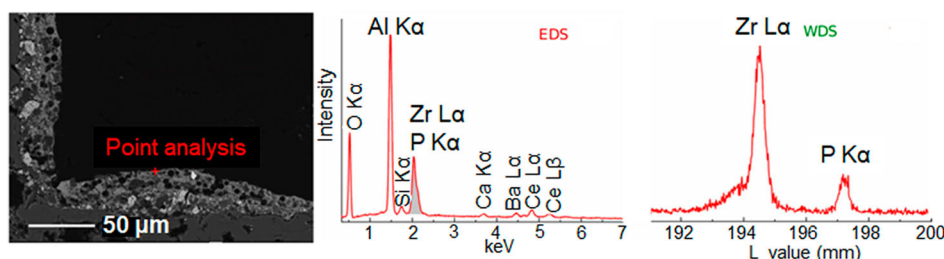


**FIGURE 10** Comparative signals from EPMA-EDS and EPMA-WDS at the same point in the automotive exhaust honeycomb sample. EDS is incapable of differentiating between Zr Ka and P Ka while in the WDS they are clearly separated. Adapted from Bian et al.<sup>[45]</sup> Copyright Elsevier (2024).

compared to EDS, which has an energy resolution of approximately 130 eV.

The full integration of energy-dispersive X-ray spectrometry (EDS) and wavelength-dispersive spectrometry (WDS) signals allows for the simultaneous collection of quantitative data for major, minor, and trace elements at a single analysis point. EPMA has been applied to measure trace elements in a wide range of materials, such as gold,<sup>[60]</sup> basaltic glasses,<sup>[61,62]</sup> olivine,<sup>[63]</sup> and  $\text{Fe}^{3+}/\text{Fe}$ ,<sup>[64]</sup> in spinel and quartz.<sup>[65]</sup>

An effective measurement framework maximizes accuracy. However, even in the field of geology, research that primarily focuses on the uncertainties quantification

is rare. Its limited sensitivity when applied to trace elements (10 ppm) with sufficient precision has been problematic.<sup>[33]</sup>

Some analysts boost the beam current or extend the analytical time to enhance the detection limit. Although these steps may improve the resolution, the impact of the high-energy electron beam concentrated in a small volume damages the sample volume. Consequently, the energy of the electron beam generates heat, increasing the sample's surface temperature, which may compromising its chemical stability (especially in samples with low thermal conductivity). Damage is associated with dehydration, heating, and evaporation or

migration of the components, resulting in inaccurate measurements of the elements. One measure to mitigate this effect is to increase the diameter of the electron beam, but this reduces the spatial resolution.<sup>[66]</sup>

## 5 | PERSPECTIVES

EPMA is a method for quantitative chemical analysis at the microscopic level. Recent advances have enhanced its precision, spatial resolution, and sensitivity through innovations in electron beam focusing and improvements in X-ray detector technology. Improving the spatial resolution has reduced the accelerating voltage requirement and, as a result, trace element analysis has improved.

Despite being well-established, it faces challenges improving precision and accuracy. Due to the sensitivity of some matrices to electron beam irradiation, there is a loss of X-ray intensity over time. The effects of certain alkaline elements during electron beam bombardment have been investigated for decades to improve quantification precision since some elements have been on-peak spectral interference.<sup>[3,5,22]</sup> Other advances include correcting for spectral interference and time dependent variations related to sensitive materials and time dependent corrections of the beam.<sup>[67]</sup>

Trace element analysis remains a challenge for the EPMA technique. The development of accurate measurement analytical methods is necessary to determine detection limits and analysis parameters to avoid overlapping spectral lines. Another critical point to be considered is the selection of primary standards with the same chemical and structural composition as the sample to be analyzed, which makes it possible to minimize matrix effects. Standard-less approaches can be applied to overcome these restrictions, in which X-ray intensities are computed and employed as virtual standards. Several studies have demonstrated encouraging outcomes when Monte Carlo simulations calculate X-ray intensities. These simulations have also effectively handled complicated analysis in non-conventional samples.<sup>[68]</sup> Other significant advances in the development of instrumentation, allowing EPMA to be successfully used for trace element analysis, include improved stability of spectrometers and the electron column when operated with high probe currents, development of new crystal monochromators with larger areas, spectrometers with ultra-high count rates, powerful software packages, and SXES.<sup>[3,13,33,66,69]</sup>

Advances in electron optics, detector technologies, and data analysis algorithms have positioned EPMA to surmount current challenges and significantly enhance its applicability in established and emerging scientific fields.

The technique's adaptability in handling complex samples and trace element analysis, combined with increasing accuracy, ensures that EPMA will remain a fundamental tool in micro-chemical material characterization. New possibilities for integrating artificial intelligence to interpret data and minimize errors, along with machine learning, pave the way for automating and refining analytical processes. As a result, the continuous evolution of EPMA provide insight into the properties and composition of materials, driving progress in sectors ranging from renewable energy and catalysis to planetary science and archaeology.<sup>[5,33,64]</sup> However, in the past 10 years, there have been significant advances in the development of instrumentation, allowing EPMA to be successfully used for trace element analysis (down to 10 ppm).

## 6 | CONCLUSIONS

EPMA has established itself as an essential tool for the micro-chemical characterization of solid materials, offering high spatial resolution and non-destructive analysis. Over the last few years, significant advances in electronic components, optical systems, and software have improved the method's precision, sensitivity, and spatial resolution, broadening its application beyond the standard geological and material science applications to include more chemistry, physics, and, in the near future, chemical engineering.

Despite these advances, the technique still faces challenges concerning the analysis of non-conductive materials and limited sensitivity for trace elements and retained noble gases. The future of EPMA lies in the constant improvement of hardware and software, more robust analytical methodologies, and optimization of matrix correction models.

## AUTHOR CONTRIBUTIONS

**Viviane de Oliveira Campos:** Conceptualization; investigation; writing – original draft; methodology; validation; visualization; writing – review and editing; formal analysis; project administration; supervision; data curation.

**Felipe Fernandes Barbosa:** Conceptualization; writing – original draft; methodology; validation; visualization; writing – review and editing; formal analysis; data curation; investigation. **Ellen Kadja Lima de Moraes:** Writing – original draft; writing – review and editing; investigation. **Dulce Maria Araújo Melo:** Writing – original draft; writing – review and editing; supervision; validation.

**Jildimara de Jesus Santana:** Conceptualization; investigation; writing – original draft; writing – review and editing; visualization; validation; methodology; project administration; formal analysis; data curation. **Gregory**



**S. Patience:** Conceptualization; investigation; writing – original draft; writing – review and editing; visualization; validation; methodology; formal analysis; project administration; supervision; data curation; resources.

## PEER REVIEW

The peer review history for this article is available at <https://www.webofscience.com/api/gateway/wos/peer-review/10.1002/cjce.25712>.

## DATA AVAILABILITY STATEMENT

The data that support the findings of this study are available from the corresponding author upon reasonable request.

## ORCID

Gregory S. Patience  <https://orcid.org/0000-0001-6593-7986>

## REFERENCES

- [1] International Standard, *Microbeam Analysis —Electron Probe Microanalysis (EPMA) 2017, ISO 23833*, Geneva, Switzerland **2017**.
- [2] Z. Deng, J. Hu, R. Liu, Y. Lv, *At. Spectrosc.* **2022**, *43*, 201.
- [3] D. Yang, Q. Yang, W. Ma, X. Ma, S. Wang, Y. Lei, *Sep. Purif. Technol.* **2023**, *308*, 1.
- [4] C. Colliex, *C. R. Phys.* **2019**, *20*, 746.
- [5] M. Liu, X. Tan, *J. Anal. Chem.* **2022**, *77*, 1333.
- [6] M. Vijayakumar, V. R. Rao, P. Angelo, *Def. Sci. J.* **1989**, *39*, 13.
- [7] R. Castaing, A. Guinier, *Proceedings of the 1st International Conference on Electron Microscopy*, Martinus Nijhoff, Delft **1950**, p. 60.
- [8] R. Castaing, *Adv. Electron. Electron Phys.* **1960**, *13*, 317.
- [9] X. Llovet, A. Moy, P. T. Pinard, J. H. Fournelle, *Prog. Mater. Sci.* **2021**, *116*, 100673.
- [10] G. S. Patience, *Can. J. Chem. Eng.* **2018**, *96*, 2312.
- [11] L. V. Hoecke, D. Boeye, A. Gonzalez-Quiroga, G. S. Patience, P. Perreault, *Can. J. Chem. Eng.* **2023**, *101*, 545.
- [12] É. Thibault, M. Chioua, M. McKay, M. Korbel, G. S. Patience, P. R. Stuart, *Can. J. Chem. Eng.* **2023**, *101*, 6055.
- [13] E. Pahija, S. Hwangbo, T. Saulnier-Bellemare, G. S. Patience, *Can. J. Chem. Eng.* **2024**, *102*, 3308.
- [14] M. F. González, N. Saadatkhah, G. S. Patience, *Can. J. Chem. Eng.* **2024**, *102*, 2004.
- [15] T. E. Davies, H. Li, S. Bessette, R. Gauvin, G. S. Patience, N. F. Dummer, *Can. J. Chem. Eng.* **2022**, *100*, 3145.
- [16] M. O. Guerrero-Pérez, G. S. Patience, *Can. J. Chem. Eng.* **2020**, *98*, 25.
- [17] Y. Zhang, L. Tang, Y. Wang, J. Wang, J. Zhou, J. Lu, Y. Zhang, Z. Zhang, *Mater. Today Commun.* **2022**, *38*, 107782.
- [18] B. Lewis, W. Thompson, F. Iglesias, *Def. Sci. J.* **2012**, *2*, 515.
- [19] S. Dushman, *Rev. Mod. Phys.* **1930**, *2*, 381.
- [20] J. Pinos, Š. Mikmeková, L. Frank, *J. Microsc.* **2017**, *266*, 335.
- [21] W. H. Bragg, W. L. Bragg, *Proc. R. Soc. London* **1913**, *88*, 428.
- [22] Y. G. Lavrentév, N. S. Karmanov, L. V. Usova, *Russian Geology and Geophysics* **2015**, *56*, 1154.
- [23] N. Braid, A. Béchu, J. C. de Souza Terra, G. S. Patience, *Can. J. Chem. Eng.* **2020**, *98*, 628.
- [24] F. Adams, C. Barbante, in *Modern Physical Metallurgy and Materials Engineering*, Elsevier, Amsterdam, The Netherlands **2015**, p. 269.
- [25] M. Takakura, T. Murano, S. Koshiya, P. McSwiggen, V. Robertson, *Microsc. Microanal.* **2022**, *28*, 1014.
- [26] H. Takahashi, T. Murano, M. Takakura, S. Asahina, M. Terauchi, M. Koike, T. Imazono, M. Koeda, T. Nagano, *IOP Conf. Ser.: Mater. Sci. Eng.* **2016**, *109*, 1.
- [27] T. Claus, J. Bünger, M. Torrilhon, *Mathematical and Computational Applications* **2021**, *26*, 1.
- [28] J. Laigo, F. Christien, R. L. Gall, F. Tancret, J. Furtado, *Mater. Charact.* **2008**, *59*, 1580.
- [29] S. J. B. Reed, *Electron Microprobe Analysis and Scanning Electron Microscopy in Geology*, Cambridge University Press, Cambridge **2005**.
- [30] P. Schweizer, E. Brackx, P. Jonnard, *X-Ray Spectrom.* **2022**, *51*, 403.
- [31] S. Imashuku, K. Wagatsuma, *Miner. Eng.* **2021**, *173*, 1.
- [32] M. I. Pownceby, C. M. MacRae, N. C. Wilson, *Miner. Eng.* **2007**, *20*, 444.
- [33] V. G. Batanova, A. V. Sobolev, V. Magnin, *IOP Conf. Ser.: Mater. Sci. Eng.* **2018**, *304*, 012001.
- [34] N. J. van Eck, L. Waltman, *Scientometrics* **2010**, *84*, 523.
- [35] C. Analytics, Web of (S)cienceTM (C)ore (C)ollection **2024**, <http://apps.webofknowledge.com> (accessed: May 2024).
- [36] Z. Han, C. Tang, J. Wang, L. Li, C. Li, *J. Catal.* **2021**, *394*, 236.
- [37] Y. Dai, P. Lu, Z. Cao, C. T. Campbell, Y. Xia, *Chem. Soc. Rev.* **2018**, *47*, 4314.
- [38] L. Jolivet, V. Motto-Ros, L. Sorbier, T. Sozinho, C. P. Lienemann, *J. Anal. At. Spectrom.* **2020**, *35*, 896.
- [39] F. Robaut, A. Crisci, M. Durand-Charre, D. Jouanne, *Microsc. Microanal.* **2006**, *12*, 331.
- [40] P. Moraille, Z. Abdali, M. Ramkaran, D. Polcari, G. S. Patience, N. D. Courchesne, A. Badia, *Can. J. Chem. Eng.* **2022**, *100*, 2778.
- [41] B. Liu, H. Nakatani, M. Terano, *J. Mol. Catal. A: Chem.* **2002**, *184*, 387.
- [42] R. Wang, Y. Gong, P. Wang, A. Zheng, Z. Wang, Y. Sha, Q. Jiang, M. Xin, D. Cao, H. Song, W. Lin, *Addit. Manuf.* **2024**, *79*, 1.
- [43] B. Xu, Z. Luo, T. Tao, Y. Wang, *Sep. Purif. Technol.* **2024**, *334*, 1.
- [44] Q. N. Dao, E. On, S. Ramadhani, K. Lee, H. Sohn, S. H. Choi, S. Y. Lee, H. Jeong, Y. Kim, *Int. J. Hydrogen Energy* **2024**, *22*, 1284.
- [45] L. Bian, C. Hu, Q. Cao, *Anal. Chim. Acta* **2024**, *1292*, 1.
- [46] X. Liu, J. Qiao, Y. Wu, X. Liu, X. Bian, *J. Alloys Compd.* **2005**, *388*, 83.
- [47] Q. Shi, Y. Huo, T. T. Berman, B. Ghaffari, M. Li, J. Allison, *Scripta Mater.* **2021**, *190*, 97.
- [48] H. Cheng, B. Leng, K. Chen, Y. Jia, J. Dong, Z. Li, X. Zhou, *Corros. Sci.* **2015**, *97*, 1.
- [49] Y. G. Lavrentév, L. V. Usova, M. Y. Lavrentév, N. S. Karmanov, *J. Anal. Chem.* **2020**, *75*, 902.
- [50] M. Eren, M. Palvanov, *Carbonates Evaporites* **2024**, *39*, 90.
- [51] Y. Gao, L. Zhanga, L. Bagas, K. Hattori, M. Liu, H. Wu, Y. Wang, Z. Chene, X. Zhao, Y. Zhang, G. Wu, *Ore Geol. Rev.* **2024**, *167*, 1.



- [52] C. F. Wust, M. A. M. Rizzi, L. Takehara, G. N. Queiroga, T. J. Girelli, F. C. Junior, *J. South Am. Earth Sci.* **2024**, 135, 1.
- [53] Z. Fan, H. Zhou, X. Wang, J. Song, J. Shi, C. Liu, J. Chen, *J. Mater. Sci.* **2024**, 31, 1.
- [54] S. Choi, J. Choi, C. Park, *Appl. Phys. B: Lasers Opt.* **2023**, 129, 8.
- [55] H. Ma, J. Henderson, J. Evans, Q. Ma, J. Cui, *J. Archaeol. Sci.* **2021**, 131, 1.
- [56] R. E. Smallman, R. J. Bishop, in *Modern Physical Metallurgy and Materials Engineering*, Butterworth-Heinemann, Oxford **1999**, p. 125.
- [57] A. C. Dunham, F. C. F. Wilkinson, *X-Ray Spectrom.* **1978**, 7, 50.
- [58] J. J. Friel, C. E. Lyman, *Microsc. Microanal.* **2006**, 12, 2.
- [59] P. Lanari, A. Vho, T. Bovay, L. Airaghi, S. Centrella, *J. Geol. Soc.* **2019**, 478, 39.
- [60] C. Gauert, M. Schannor, L. Hecht, M. Radtke, U. Reinholz, *Geostand. Geoanal. Res.* **2016**, 40, 267.
- [61] C. Zhang, J. Koepke, L. Wang, P. E. Wolff, S. Wilke, A. Stechern, R. Almeev, F. Holtz, *Geostand. Geoanal. Res.* **2016**, 40, 351.
- [62] M. Gavrilenko, G. V. Batanova, X. Llovet, S. Krashennnikov, N. A. Koshlyakova, V. A. Sobolev, *Chem. Geol.* **2023**, 621, 1.
- [63] D. Zamboni, J. Trela, E. Gazel, A. V. Sobolev, C. Cannatelli, F. Lucchi, V. Batanova, B. D. Vivo, *Lithos* **2017**, 272, 185.
- [64] L. Jia, Y. Chen, Q. Mao, D. Zhang, J. Yuan, X. Li, S. Wu, D. Zhang, *At. Spectrosc.* **2022**, 43, 42.
- [65] A. S. Shah, Y. Shao, Y. Zhang, H. Zhao, L. Zhao, *Minerals* **2022**, 12, 1.
- [66] L. P. He, L. X. Huang, L. hang, *Solid Earth Sci. Libr.* **2024**, 9, 1.
- [67] J. J. Donovan, J. M. Allaz, A. von der Handt, G. G. Seward, O. Neill, K. Goemann, J. Chouinard, P. K. Carpenter, *American Mineralogist* **2021**, 106, 1717.
- [68] J. Donovan, P. Pinard, H. Demers, *Microsc. Microanal.* **2019**, 25, 735.
- [69] W. Ma, G. Zhu, H. L. a, Z. Meng, K. Zhang, K. Yan, Y. Yang, Z. Li, J. Zhang, C. Wang, *J. Cleaner Prod.* **2023**, 423, 138669.

**How to cite this article:** V. de Oliveira Campos, F. F. Barbosa, E. K. L. de Moraes, D. M. A. Melo, J. de Jesus Santana, G. S. Patience, *Can. J. Chem. Eng.* **2025**, 103(7), 3000. <https://doi.org/10.1002/cjce.25712>